Systematic compositional changes and their influence on lattice and optoelectronic properties of Cu2ZnSnSe4 kesterite solar cells

J. Márquez*[1], M. Neuschitzer[2], M. Dimitrievska[2], Rene Gunder[3,5], S. Haass[4], M. Werner[4], Y. E. Romanyuk[4,] S. Schorr[3,5], N. M. Pearsall[1] and I. Forbes[1]

*Corresponding author: jose.prieto@northumbria.ac.uk;

Telephone: +44 7455 773070

1. Northumbria Photovoltaic Applications Group, Department of Physics and Electrical Engineering, Northumbria University, Newcastle upon Tyne, UK

2. Catalonia Institute for Energy Research (IREC), C. Jardins de les Dones de Negre 1, 08930 Sant Adrià del Besòs, Barcelona, Spain

3. Helmholtz-Zentrum Berlin for Materials and Energy, Hahn-Meitner-Platz 1, 14109 Berlin, Germany

4. Empa – Swiss Federal Laboratories for Materials Science and Technology, Laboratory for Thin Films and Photovoltaics, 8600 Dübendorf, Switzerland

5. Free University Berlin, Institute of Geological Sciences, Malteserstr.74-100, Berlin, Germany

Kesterite thin films solar cells have been studied in recent years as a potential earth abundant alternative to other thin film technologies such as the ones based on the chalcopyrite Cu(In,Ga)Se_2 (CIGS). However, the efficiency of the kesterite devices is still low and needs further development. In order to increase the performance of the kesterite solar cells, a better understanding of the influence of variations of compositions on the crystal lattice of the absorber layer is needed. This paper presents a study of how variations in the Cu content in the $Cu_2ZnSnSe_4$ (CZTSe) absorber layer affects the crystal structure and therefore changes the optoelectronic properties of the solar cell. Three sets of CZTSe absorbers with different Cu content were synthesised by sputtering of metallic targets followed by a rapid thermal selenisation process. An accurate characterisation of the lattice parameters of the unit cell is presented, showing that a decrease of the Cu content in the CZTSe absorber layer diminishes the unit cell volume. This decrease in volume is related to an increase in the concentration of [V_{Cu} + Zn_{Cu}] and the ordering of the Cu/Zn atoms in the (001) plane. The variations in the lattice of CZTSe induced by decreasing the Cu content cause an increase of the bandgap of absorber layer, which leads to an increase of the open circuit voltage (V_{OC}) in the devices. The best solar cell was based on the absorber layer with the lowest Cu content

and yielded an efficiency of 8.1% with a fill factor of 59.8 %, Jsc = 31.1 mA/cm2 and Voc = 434 mV.

1. Introduction

Thin film solar cells based on $Cu_2ZnSn(S,Se)_4$ (CZTSSe) have been studied as an alternative to $Cu(In,Ga)Se_2$ (CIGSe). To date, the highest efficiency achieved has been 12,6% [1]. However, it has been suggested that small area devices need to reach an efficiency of 19% in order to justify commercial manufacture at a significant level [2]. Currently the material presents many barriers that need to be better understood in order to continue increasing the performance of CZTSSe based solar cells. The open circuit voltage (V_{OC}) deficit, defined as $Eg/q - V_{OC}$, is substantially larger for CZTSSe devices than for good CIGSe devices which generally present V_{OC} deficits lower than 500 mV [3]. There are several possible explanations for the V_{OC} deficit that CZTSSe devices currently present. Firstly, $Cu_2ZnSnSe_4$ (CZTSe) and Cu_2ZnSnS_4 (CZTS) present a very narrow stoichiometric region [4-6]. In addition, it has been demonstrated that at high temperatures, when in contact with metallic Mo which is normally used for the back contact in kesterite solar cells, CZTSSe decomposes [7, 8]. It has also been proven that high chalcogen partial pressures are required when crystallising the CZTSSe in order to avoid the decomposition of the absorber layer on the surface [9] that leads to a decrease in the photovoltaic performance of the devices. In the bulk of the absorber layer, many questions are still to be resolved regarding the crystal structure of these materials. A better understanding of the formation and impact of defects needs to be developed in order to decrease the current V_{OC} deficit of the best kesterite devices [10]. A combination of neutron and X-ray diffraction analysis demonstrated that CZTSe and CZTS crystallises in the kesterite type structure and also that Cu_{Zn} and Zn_{Cu} antisites in the (001) planes at z = 1/4 and 3/4 are present in high concentration opening the discussion of how ordered are the synthesized kesterite type compounds [11]. The order-disorder transition has been studied by Scragg *et al.* for CZTS [12], Kraemmer *et al.* for CZTSSe [13], and Redinger *et al.* and Rey *et al.* for CZTSe [14]. It has been concluded that this transition can change the effective bandgap of the material by more than 100 meV, thus affecting the Voc of solar cells synthesized from the same absorbers with different degrees of ordering. [15].

It has been reported several times in the literature that Cu-poor and Zn-rich compositions are needed to make high efficiency solar cells, although more experimental data regarding composition is needed in order to determine how the variation in the metal ratios affects the crystal structure of CZTSSe compounds in thin films and the correlation with the optoelectronic properties of the solar cells processed from them. When different publications where solar cells and their compositions are reported are compared, it is difficult to identify trends and therefore difficult to conclude why the devices work better within certain values of composition. If we also add errors in the compositional

measurements, different calibration methods, and different techniques used for measuring, it is even more difficult to define certain values of compositions and relate them to the properties of the solar cells.

First principle calculations have explained theoretically why Cu-poor, Zn-rich kesterite solar cells should be of higher efficiency[16]. It was concluded that V_{Cu} could contribute to p-type conductivity. It was also shown that some self-compensated defect clusters [V_{Cu} + Zn_{Cu}], [Zn_{Sn} + 2Zn_{Cu}] and [2Cu_{Zn} + Sn_{Zn}] have low formation energy and can be present in high population either in CZTS and in CZTSe. [2Cu_{Zn} + Sn_{Zn}] could induce electron-trapping effects and [V_{Cu} + Zn_{Cu}] could induce a downshift in the valence band that might be beneficial for the solar cell performance, helping the electron-hole separation.

Lafond et al. studied the most realistic substitution reactions for Cu-poor CZTS concluding that two types of defects were the most likely to be formed: [Zn^{2+} + V_{Cu}] (A-type, presenting Cu poor and Zn rich composition) and [2Zn^{2+}_{Cu} + Zn^{2+}_{Sn}] (B-type, presenting Cu poor and Sn poor composition) [17]. In a solid state nuclear magnetic resonance (NMR) study, Paris *et al.* demonstrated the presence of [V_{Cu} + Zn_{Cu}] and [2Zn^{2+}_{Cu} + Zn^{2+}_{Sn}] for A-type and B-Type CZTS respectively [18].

In this paper we present an investigation of the influence of the metal ratios on the properties of Cu poor CZTSe thin films absorber layers and also demonstrate how the variations in composition affect the properties of CZTSe solar cells, with the aim of improving the understanding of why Cu-poor Zn-rich compositions are also needed in CZTSSe for synthesising high efficiency solar cells.

2. Experimental

2.1. CZTSe absorber synthesis

Sets of Cu-Zn-Sn (CZT) multilayer precursor films were deposited using a Nordiko 2000 magnetron sputter deposition system with 150 mm diameter, high purity (5N) elemental targets. Molybdenum coated soda-lime glass substrates were used in all cases. Power values of 70 W and 140 W were applied to the Zn and Sn targets, respectively. Three sets of precursor were prepared by varying only the power of the Cu target resulting in CZT precursors with different Cu content. The power applied to the Cu target was 130 W, 120 W, and 110 W for the films presented in this study. For the CZT precursor deposition, the Argon pressure was $3x10^{-3}$ Torr (0.4 Pa) and the deposition time was adjusted to achieve around 450 nm CZT precursor films. The precursors were then introduced into graphite boxes together with 4 Se pellets. The graphite boxes containing the precursors and the Se pellets were then heated in a Rapid Thermal Processor (Annealsys AS-One)

at 300 °C and 500 °C for 5 and 15 minutes respectively. The rate of the ramp for both steps was 4 °C per second. The process was carried out under 85 kPa of N_2 base pressure.

2.2. CZTSe absorber characterisation

The CZTSe absorbers were measured with a PANalytical X'Pert MPD Pro X-ray diffractometer in grazing incidence (GI) configuration at incident angels of 0.5, 1, and 2º using a Cu K-α radiation source (λ=0.15406 nm). Le Bail refinements of the patterns were performed using the Fullprof software package in order to determine the lattice constant values [19]. The composition of the samples was determined using a FEI Quanta 200 scanning electron microscope (SEM) equipped with an Oxford Instruments energy dispersive X-ray analyser (EDX) and X-ray fluorescence (XRF) with an operating voltage of 40kV. The EDX system was calibrated using standards for quantitative analysis recommended by Oxford Instruments. The software used to perform the calibration was the Quant Optimization which is part of the INCA software package for EDX analysis. The XRF system was calibrated with reference samples measured by inductively coupled plasma mass spectrometry (ICP-MS). Raman scattering measurements were performed with 532.0 nm excitation using a LabRam HR800-UV, and 457.9 nm excitation a with T64000 Horiba-Jobin Yvon spectrometers.

2.3. Device fabrication and characterisation

CZTSe absorbers were etched with 10 %w KCN solution for 30 seconds. A CdS buffer layer of approximately 50nm in thickness was deposited after the etching treatment by chemical bath deposition (CBD) followed by an i-ZnO/ZnO:Al window layer deposited by RF sputtering. 0.028 M of cadmium acetate and 0.374 M thiourea aqueous solutions were used as the Cd and S sources respectively in the CBD process. The total volume of the solution was 0.25L. Cells of area 0.09 cm^2 were mechanically scribed. Illuminated J-V curves were measured under 100mW/cm^2 simulated AM1.5 solar illumination calibrated with a Si reference cell and external quantum efficiency (EQE) was measured using a lock-in amplifier and a chopped white light source (900 W, halogen lamp, 360 Hz) combined with a dual grating monochromator. The sun simulator has an UXL 553 Short arc Xenon lamp. The spectrum is matched by an AM1.5G filter and meets the class "A" standard. Both EQE and J-V measurements were performed by contacting the front contact of the solar cells directly on the TCO, since there was no metallic grid added.

3. Results and discussion

3.1. Synthesis of absorbers and characterisation

Cu-Zn-Sn metallic precursor layers were deposited on Mo coated SLG glasses as described in the experimental section. Three different compositions of precursors were used for this study. To show a clear comparison, the metal compositions of the absorber layers produced in this study are plotted in Figure 1 in the pseudo-ternary phase diagram (TPD) reported by Dudchak et al [4]. The metal atomic composition of the precursors and absorber layers was measured either by EDX at 20 kV from the top view or with XRF, and the values can be seen in Table 1. For an easier understanding of the manuscript, the samples prepared with the three different compositions will be referred as Sample 1, Sample 2 and Sample 3 as the Cu/(Zn+Sn) ratio decreases in the films and the composition moves away from the stoichiometric point in the TPD. A comparison of the composition between the precursors and the absorbers measured by XRF shows that the Cu/(Zn+Sn) ratios increase after the selenisation process. We attribute this to the loss of Zn and Sn due to the formation of volatile compounds of both constituents [20]. The Zn/Sn ratios seen for Sample 2 and Sample 3 increase after the selenisation process, indicating an increase of the Sn loss as the Cu content decreases in the precursor, as also observed by Collord et al [21].

In previous studies, we have found that EDX compositional measurements could be influenced by the presence of secondary phases on the surface such as ZnSe or Cu_xSe providing values that do not necessarily correspond to a representative average composition of the absorber layer [22]. Therefore, a combination of EDX and XRF measurements could be useful to compare and especially to make sure that the trends of composition studied are consistent. We observe differences between the two measurements. Apart for the difference in penetration depth of each technique, this variation could be attributed to several factors such as the calibration used for each method. The main difference observed between the measurements is that, for the samples of this study, in both the precursors and the absorbers, the apparent Cu content is higher when measuring with XRF. The average composition of the films measured with the two techniques follows the same variation, with the difference between them being the variation in Cu content. Qualitatively, it is possible to observe that “Sample 2” and “Sample 3” have compositions far from the stoichiometric region. The reactive annealing process used for the synthesis of the CZTSe absorbers uses fast ramping rates. This ternary phase diagram, which applies to equilibrium conditions at 400 ºC, might not be the most adequate tool for estimating the amount and presence of secondary phases in the film. However, it can provide an idea of which potential secondary phases might be present in the absorber layer and is useful for the clarity of the reader. As the Cu content in the film decreases, the compositions plotted in the TDP are located in the

ZnSe-$SnSe_2$-CZTSe region so one could predict the possible presence of ZnSe and $SnSe_x$ particularly in "Sample 2" and "Sample 3".

3.2. Secondary phases and microstructure

The metal compositions of the samples are plotted along the off-stoichiometric type lines in Figure 2b. As the Cu decreases from Sample 1 to Sample 3, the points move towards the A-type line, predicting an increased in the concentration of $[V_{Cu} + Zn_{Cu}]$[17]. Raman spectra of the CZTSe absorbers synthesised measured with 532nm excitation are shown in Figure 2b. All peaks observed in the spectra are attributed to the Raman modes of the CZTSe phase [23]. For the analysis presented here, we will refer to two main peaks:

1) The most intense peak centred at 197 cm^{-1} which is attributed to A symmetry mode and involves purely Se anion vibrations [24].
2) A broad peak centred at around 170 cm^{-1} which could be attributed to the convolution of two A modes (corresponding to Se vibrations) and two B modes (involving mostly Cu/Zn and Cu/Sn atomic plane vibrations [25])

The three spectra are normalised to the most intense peak at 197 cm^{-1}. When the Cu content is decreased in the absorber layers, the relative intensity of the peak at 170 cm^{-1} decreases. It was previously observed that the intensity of this peak with respect to the A mode at 197 cm^{-1} was very sensitive to the Cu content in CZTSe thin films, particularly when there was Cu deficit in the structure [26]. When the Cu/(Zn+Sn) ratio decreases and the composition moves away from the stoichiometric point towards the Cu poor region in the TPD shown in Figure 1, the relative intensity of the band at 170 cm^{-1} also decreases. One possible explanation for this decrease is that it is related to an increase in the concentration of $[V_{Cu} + Zn_{Cu}]$, which has been theoretically predicted to be present in high population in Cu poor CZTSe [16]. This could decrease the intensity of the B modes appearing in this region corresponding to the vibrations of Cu/Zn and Cu/Sn atomic vibrations, as reported in [23], which would lead to the overall decrease in the intensity of the peak cantered at 170 cm^{-1}. The inset in Figure 2b shows a magnification of the A mode at 196 cm^{-1}. When looking in detail at the position of this peak, one can observe that for "Sample 2" and "Sample 3" it is blue shifted in comparison to "Sample1". Rey *et al*. observed a blue shift of the A mode that could be related to an increase in the ordering in the samples of their study. [14]. In our study, this could be an indication that the two CZTSe thin films with less Cu content are more ordered than the one with composition near to the stoichiometric point. This is in agreement with the study of Paris *et al.* where they observed

that Cu poor CZTS samples with predominant [V_{Cu} + Zn_{Cu}] defect clusters presented an increase in the ordering of the Cu and Zn cations in the 2c and 2d positions [18].

Le Bail analysis was performed on the XRD patterns acquired at different GI angles for the CZTSe absorbers. The diffractograms acquired at a GI angle of 1° are shown in Figure 3. No secondary phases could be detected with this technique in the absorbers of this study. This is particularly interesting, since the composition of "Sample 2" and "Sample 3" are far away from the stoichiometric region of CZTSe and, if there was a quantitative presence of $SnSe_x$, then this technique should indicate it. The diffraction patterns were measured with low incidence angle of 0.5, 1 and 2º acquiring information from the near surface and bulk region of the absorbers. This allowed us to reduce the potential variations in the lattice parameter calculations induced by uniform strain created by the growth of $MoSe_2$ at the interface with the back contact. In addition, the acquisition of data from the near surface region ensures a more reliable comparison with the penetration depth of the laser used for recording the Raman spectra (~100nm). Figure 4 shows a comparison of the lattice parameters obtained for the CZTSe absorber layers of this study. The lattice constant *a* does not appear to be influenced by the variations in composition, although the lattice constant *c* decreases significantly when the Cu content in the samples is decreased. Schorr studied the temperature behaviour of the lattice parameters of (CZTS), where a monotonic decrease of the lattice parameter *a* was observed with decreasing temperature [11]. A different behaviour was observed for *c*, where a kink indicating a more abrupt reduction of the lattice constant was observed starting at around 260ºC. This temperature was estimated to be the order-disorder transition temperature of this compound [12]. Additionally, Cu/Zn disorder has been predicted to expand the unit cell volume mainly by the increase in the value of *c,* suggesting that an accurate estimation of the lattice parameters can provide valuable information related to order-disorder in CZTSSe materials. Our results show that the lower the Cu content of the CZTSe samples, the lower is the value of *c.* The decrease in the value of *c* is in agreement with the theory of the increase in ordering of Cu/Zn (001) planes, and as well as the results obtained from Raman spectroscopy.

3.3. Device performance

Current- voltage characteristics values of the best devices processed with the CZTSe absorbers with different compositions within the Cu-poor and Zn-rich region are shown in Table 2 and in Figure 5 c, d, e and f with the average and maximum values of 9 cells measured in each sample category. The dark and illuminated current density- voltage (J-V) curves

are represented in Figure 5a. It is possible to observe an increase in the performance of the devices when the Cu content in the absorber layer is decreased. This increase in performance is mainly driven by an increase in V_{OC}, from 367 mV to 434 mV. EQE measurements of the solar cells with different compositions are also presented in Figure 5b. The three devices present EQE values around 80-90 % between 500 and 900 nm. It is also possible to see interference in this range that may lead to loss in current. This is attributed to the TCO which in the case of these samples is about 700 nm thick with the aim of having a safer contact with sharp probes for electrical characterisation, since a front grid was not evaporated on these devices. The bandgap, Eg, of the devices is calculated from the inflection point of the decay of EQE at long wavelength. The values obtained are also shown in Table 2. This method has already been used in highly efficient CZTSSe solar cells for calculating the bandgap and for evaluating the tail profile associated with potential fluctuations and bandgap fluctuations. The derivative method was also assumed to be the most robust for the calculation of Eg values [27]. It is interesting to observe that a difference in the bandgap of around 70 meV can be found between Sample 1 and Sample 3. This difference can also explain the increase in V_{OC} of around 70 mV in the case of the best cells and an increase of around 50 mV in the average values as shown in Figure 5d. V_{OC} varied from 367 to 434 mV when changing composition of the best devices from Sample 1 to Sample 3, the one with the lowest Cu content of the series. A similar trend with decreasing Cu content and increasing Zn/Sn ratio has also been identified for the CZTSSe solar cells [21].

Variations in the crystal structure that CZTSSe materials adopt leads to different optoelectronic properties. In order to discuss the V_{OC} increase observed in our devices, several considerations regarding the bandgap dependency with the crystal structure of CZTSSe compounds need to be taken into account. Using different calculation methods, it is found that there could be a variation of around 150 meV between CZTSe in the kesterite or stannite crystal structure [28-30]. Rey *et al*., in an experimental study of the order-disorder transition in CZTSe co-evaporated thin films, observed an increase in bandgap from 0.94 to 1.06 eV after an ordering procedure. It is also important to consider how different point defects generated by differences in composition could induce significant differences in the bandgap. Charge compensated defect clusters have been calculated to be present in high concentration and to highly contribute to the non-stoichiometry of CZTSe. In particular $[V_{Cu} + Zn_{Cu}]$ induces a downshift of the valence band maximum and an upshift of the conduction band minimum [16].

In the previous section, it was shown that Raman and GIXRD measurements performed in the absorber layers suggest that the concentration of [V_{Cu} + Zn_{Cu}] defect clusters increases with decreasing Cu content. This increases the order in the Cu-Zn *2c* and *2d* positions, thus, increasing the Eg of the CZTSe absorber layers leading to an increase in the V_{OC} of the fabricated solar cells. In addition, while the Cu content in the CZTSe absorber layers decreases and the Zn/Sn ratio increases, in theory, it has been predicted that the concentration of [$2Cu_{Zn}$ + Sn_{Zn}] decreases, producing a downshift of the conduction band edge and inducing electron trapping, thus reducing the solar cell performance [16].

4. Conclusion

CZTSe absorber layers with a variation of Cu-poor and Zn-rich content have been synthesised in order to investigate the correlation of modifications observed in the crystal structure with the optoelectronic properties of CZTSe devices. Raman spectroscopy suggests an increase in [V_{Cu} + Zn_{Cu}] defect clusters as the [Cu/(Zn+Sn)] ratio decreases and [Zn/Sn] ratio increases. This is observed from the change in intensity of the band at around 170cm^{-1} relative to the band at 197 cm^{-1}. Le Bail analysis has been performed for the X-ray diffraction patterns of the CZTSe absorber layers in grazing incidence configuration. In the same compositional trend, while the lattice parameter *a* remains constant, *c* decreases. J-V results showed a dependence of the V_{OC} values on the Cu content ranging from 367 to 434 mV as the Cu concentration decreased in the absorbers. EQE shows that the increase in the maximum achievable V_{OC} appears to be linked to a widening of the bandgap. The best solar cell was based on the absorber layer with the lowest Cu content and yielded an efficiency of 8.1% with a fill factor of 59.8 %, J_{SC} = 31.1 mA/cm^2 and V_{OC} = 434 mV. We propose that the widening of the bandgap is attributed to an increase of the concentration of the [V_{Cu} + Zn_{Cu}] defect cluster which induces ordering in the Cu/Zn (001) planes of the CZTSe. The results observed in the series of the presented devices show a good agreement with theoretical calculations regarding the influence of the defect clusters on the optoelectronic properties of CZTSSe solar cells.

Acknowledgements

This work has been undertaken within a Marie Curie, Initial Training Network (ITN) project, "KESTCELLS" co-financed by the Seventh Framework Programme of the European Commission (FP7/2007-2013) under grant agreement n°316488. The authors would also like to acknowledge the ASC in Uppsala for providing Mo substrates for part of this study. J. M. is very thankful to Galina Gurieva, Elisa Valle-Rios and Julien Marquardt from HZB for helping with GIXRD measurements and to S. Levcenko for fruitful discussions.

References

[1] W. Wang, M.T. Winkler, O. Gunawan, T. Gokmen, T.K. Todorov, Y. Zhu, D.B. Mitzi, Device Characteristics of CZTSSe Thin-Film Solar Cells with 12.6% Efficiency, Advanced Energy Materials, (2013).

[2] I.L. Repins, M.J. Romero, J.V. Li, W. Su-Huai, D. Kuciauskas, J. Chun-Sheng, C. Beall, C. DeHart, J. Mann, H. Wan-Ching, G. Teeter, A. Goodrich, R. Noufi, Kesterite Successes, Ongoing Work, and Challenges: A Perspective From Vacuum Deposition, Photovoltaics, IEEE Journal of, 3 (2013) 439-445.

[3] J. Kim, H. Hiroi, T.K. Todorov, O. Gunawan, M. Kuwahara, T. Gokmen, D. Nair, M. Hopstaken, B. Shin, Y.S. Lee, W. Wang, H. Sugimoto, D.B. Mitzi, High Efficiency CuZnSn(S,Se) Solar Cells by Applying a Double In S /CdS Emitter, Advanced materials, (2014).

[4] I.V. Dudchak, L.V. Piskach, Phase equilibria in the Cu SnSe –SnSe –ZnSe system, Journal of Alloys and Compounds, 351 (2002) 145-150.

[5] I.D. Olekseyuk, I.V. Dudchak, L.V. Piskach, Phase equilibria in the Cu2S–ZnS–SnS2 system, Journal of Alloys and Compounds, 368 (2004) 135-143.

[6] A.J. Jackson, A. Walsh, Ab initio thermodynamic model of Cu2ZnSnS4, Journal of Materials Chemistry A, 2 (2014) 7829-7836.

[7] J.J. Scragg, T. Kubart, J.T. Wätjen, T. Ericson, M.K. Linnarsson, C. Platzer-Björkman, Effects of Back Contact Instability on Cu2ZnSnS4Devices and Processes, Chemistry of Materials, 25 (2013) 3162-3171.

[8] S. López-Marino, M. Placidi, A. Pérez-Tomás, J. Llobet, V. Izquierdo-Roca, X. Fontané, A. Fairbrother, M. Espíndola-Rodríguez, D. Sylla, A. Pérez-Rodríguez, E. Saucedo, Inhibiting the absorber/Mo-back contact decomposition reaction in Cu2ZnSnSe4 solar cells: the role of a ZnO intermediate nanolayer, Journal of Materials Chemistry A, 1 (2013) 8338.

[9] J.J. Scragg, P.J. Dale, D. Colombara, L.M. Peter, Thermodynamic Aspects of the Synthesis of Thin-Film Materials for Solar Cells, Chemphyschem : a European journal of chemical physics and physical chemistry, 13 (2012) 3035-3046.

[10] A. Polizzotti, I.L. Repins, R. Noufi, S.-H. Wei, D.B. Mitzi, The state and future prospects of kesterite photovoltaics, Energy & Environmental Science, 6 (2013) 3171-3182.

[11] S. Schorr, The crystal structure of kesterite type compounds: A neutron and X-ray diffraction study, Solar Energy Materials and Solar Cells, 95 (2011) 1482-1488.

[12] J.J.S. Scragg, L. Choubrac, A. Lafond, T. Ericson, C. Platzer-Björkman, A low-temperature order-disorder transition in Cu2ZnSnS4 thin films, Applied Physics Letters, 104 (2014) 041911.

[13] C. Krämmer, C. Huber, C. Zimmermann, M. Lang, T. Schnabel, T. Abzieher, E. Ahlswede, H. Kalt, M. Hetterich, Reversible order-disorder related band gap changes in Cu2ZnSn(S,Se)4 via post-annealing of solar cells measured by electroreflectance, Applied Physics Letters, 105 (2014) 262104.

[14] A.R. G. Rey, J. Sendler, T. P. Weiss, M. Thevenin, M. Guennou, B. El Adib, and S. Siebentritt, The band gap of Cu2ZnSnSe4: Effect of order-disorder, APPLIED PHYSICS LETTERS, (2014).

[15] M. Grossberg, J. Krustok, T. Raadik, M. Kauk-Kuusik, J. Raudoja, Photoluminescence study of disordering in the cation sublattice of Cu2ZnSnS4, Current Applied Physics, (2014).

[16] S. Chen, A. Walsh, X.G. Gong, S.H. Wei, Classification of lattice defects in the kesterite Cu2ZnSnS4 and Cu2ZnSnSe4 earth-abundant solar cell absorbers, Advanced materials, 25 (2013) 1522-1539.

[17] A. Lafond, L. Choubrac, C. Guillot-Deudon, P. Deniard, S. Jobic, Crystal Structures of Photovoltaic Chalcogenides, an Intricate Puzzle to Solve: the Cases of CIGSe and CZTS Materials, Zeitschrift für anorganische und allgemeine Chemie, 638 (2012) 2571-2577.

[18] M. Paris, L. Choubrac, A. Lafond, C. Guillot-Deudon, S. Jobic, Solid-State NMR and Raman Spectroscopy To Address the Local Structure of Defects and the Tricky Issue of the Cu/Zn Disorder in Cu-Poor, Zn-Rich CZTS Materials, Inorganic chemistry, 53 (2014) 8646-8653.
[19] J. Rodriguez-Carvajal, FULLPROF: a program for Rietveld refinement and pattern matching analysis, in: satellite meeting on powder diffraction of the XV congress of the IUCr, Toulouse, France:[sn], 1990.
[20] J.J. Scragg, T. Ericson, T. Kubart, M. Edoff, C. Platzer-Björkman, Chemical Insights into the Instability of Cu2ZnSnS4 Films during Annealing, Chemistry of Materials, 23 (2011) 4625-4633.
[21] A.D. Collord, H. Xin, H.W. Hillhouse, Combinatorial Exploration of the Effects of Intrinsic and Extrinsic Defects in Cu2ZnSn(S,Se)4, Photovoltaics, IEEE Journal of, PP (2014) 1-11.
[22] J. Márquez-Prieto, I. Forbes, Evolution of Phases in Two Stage Vacuum Processed Thin Film Cu2ZnSnSe4 Absorber Layers, Materials Research and Innovations, 18 (7) (2014) 515-518.
[23] M. Dimitrievska, A. Fairbrother, E. Saucedo, A. Pérez-Rodríguez, V. Izquierdo-Roca, Influence of compositionally induced defects on the vibrational properties of device grade Cu2ZnSnSe4 absorbers for kesterite based solar cells, Applied Physics Letters, 106 (2015) 073903.
[24] N.B. Mortazavi Amiri, A. Postnikov, Electronic structure and lattice dynamics in kesterite-type Cu2ZnSnSe4 from first-principles calculations, Physical Review B, 82 (2010) 205204.
[25] J.M. Skelton, A.J. Jackson, M. Dimitrievska, S.K. Wallace, A. Walsh, Vibrational spectra and lattice thermal conductivity of kesterite-structured Cu2ZnSnS4 and Cu2ZnSnSe4, APL Materials, 3 (2015) 041102.
[26] J. Márquez-Prieto, Y. Ren, R.W. Miles, N. Pearsall, I. Forbes, The influence of precursor Cu content and two-stage processing conditions on the microstructure of Cu2ZnSnSe4, Thin Solid Films, 582 (2015) 220-223.
[27] T. Gokmen, O. Gunawan, T.K. Todorov, D.B. Mitzi, Band tailing and efficiency limitation in kesterite solar cells, Applied Physics Letters, 103 (2013) 103506.
[28] S. Chen, X.G. Gong, A. Walsh, S.-H. Wei, Crystal and electronic band structure of Cu[sub 2]ZnSnX[sub 4] (X=S and Se) photovoltaic absorbers: First-principles insights, Applied Physics Letters, 94 (2009) 041903.
[29] C. Persson, Electronic and optical properties of Cu2ZnSnS4 and Cu2ZnSnSe4, Journal of Applied Physics, 107 (2010) -.
[30] S. Botti, D. Kammerlander, M.A.L. Marques, Band structures of Cu2ZnSnS4 and Cu2ZnSnSe4 from many-body methods, Applied Physics Letters, 98 (2011) 241915.

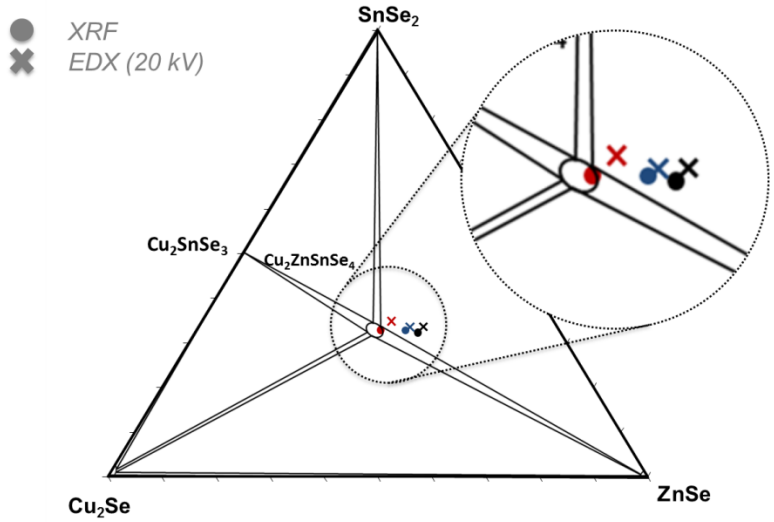

467

468 **Figure 1.** Pseudo-ternary phase diagram showing the average composition of the
469 CZTSe absorber layers of this study measured with XRF represented with dots and
470 EDX represented with crosses. As the points shift away from the stoichiometric point,
471 the Cu content decreases moving from the Sample 1 (red), to the Sample 2 (blue) and
472 then Sample 3 (black).

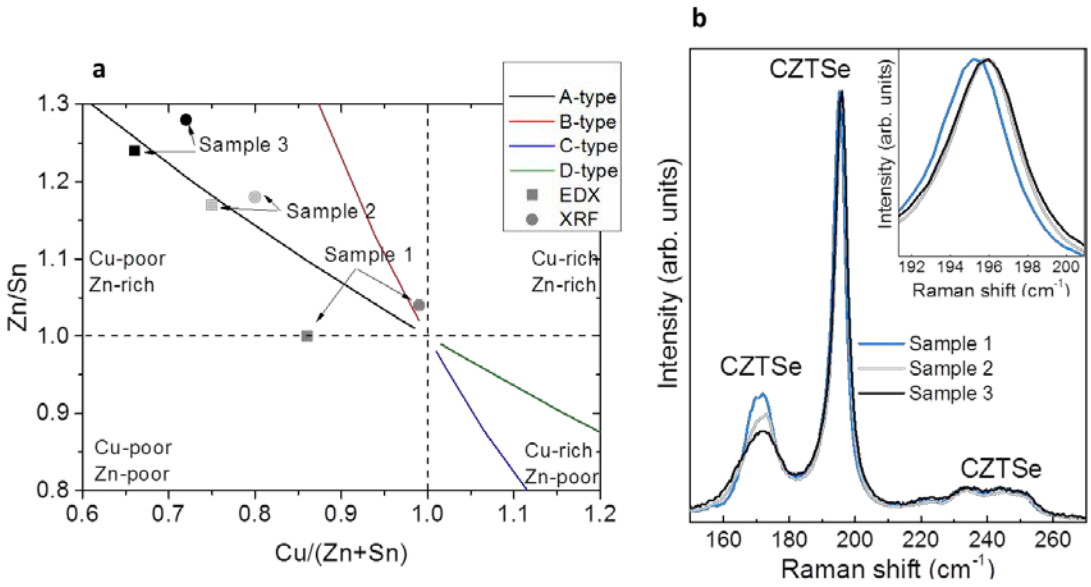

473

474 **Figure 2.** a) Positions of the samples 1-3 in the Cu/(Zn+Sn)-Zn/Sn plot indicating the
475 off-stoichiometric type. b) Raman Spectra of the Sample 1 (blue), Sample 2 (grey) and
476 Sample 3 (black) acquired with 532 nm excitation wavelength. The inset shows a
477 magnification of the main A mode at around 197 cm^{-1}.

478

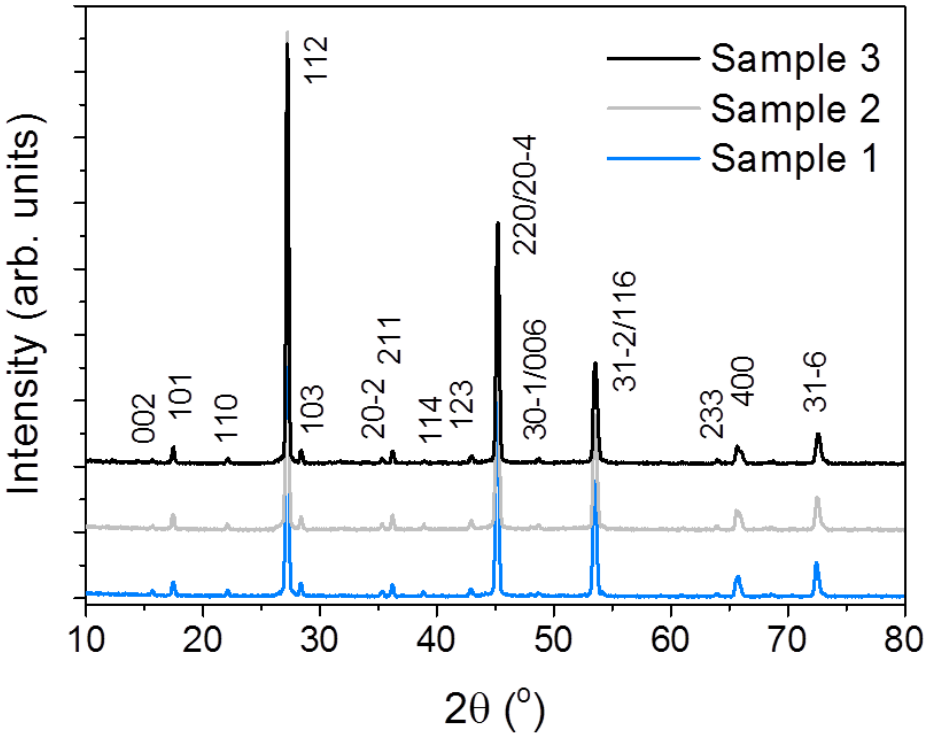

479

480 **Figure 3.** XRD patterns of Sample 1 (blue), Sample 2 (grey) and Sample 3 (black)
481 acquired for a grazing incidence angle of 1°.

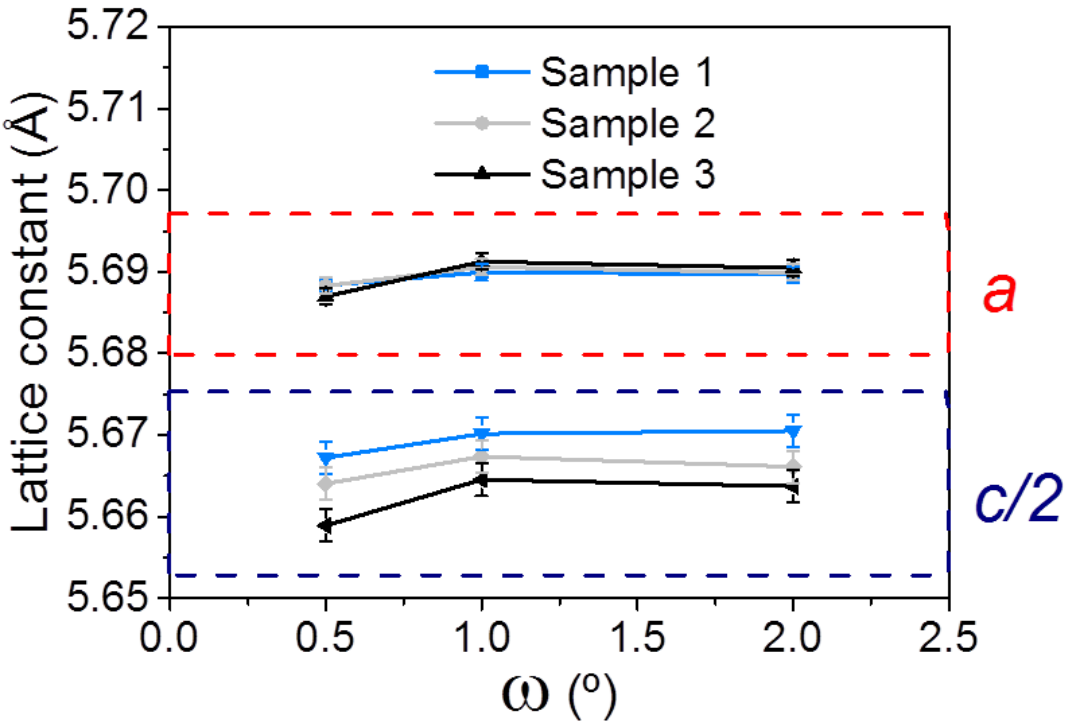

Figure 4. Lattice parameters of the of the Sample 1 (blue), Sample 2 (grey) and Sample 3 (black) CZTSe absorber layers calculated from the patterns acquired for different grazing incidence angles.

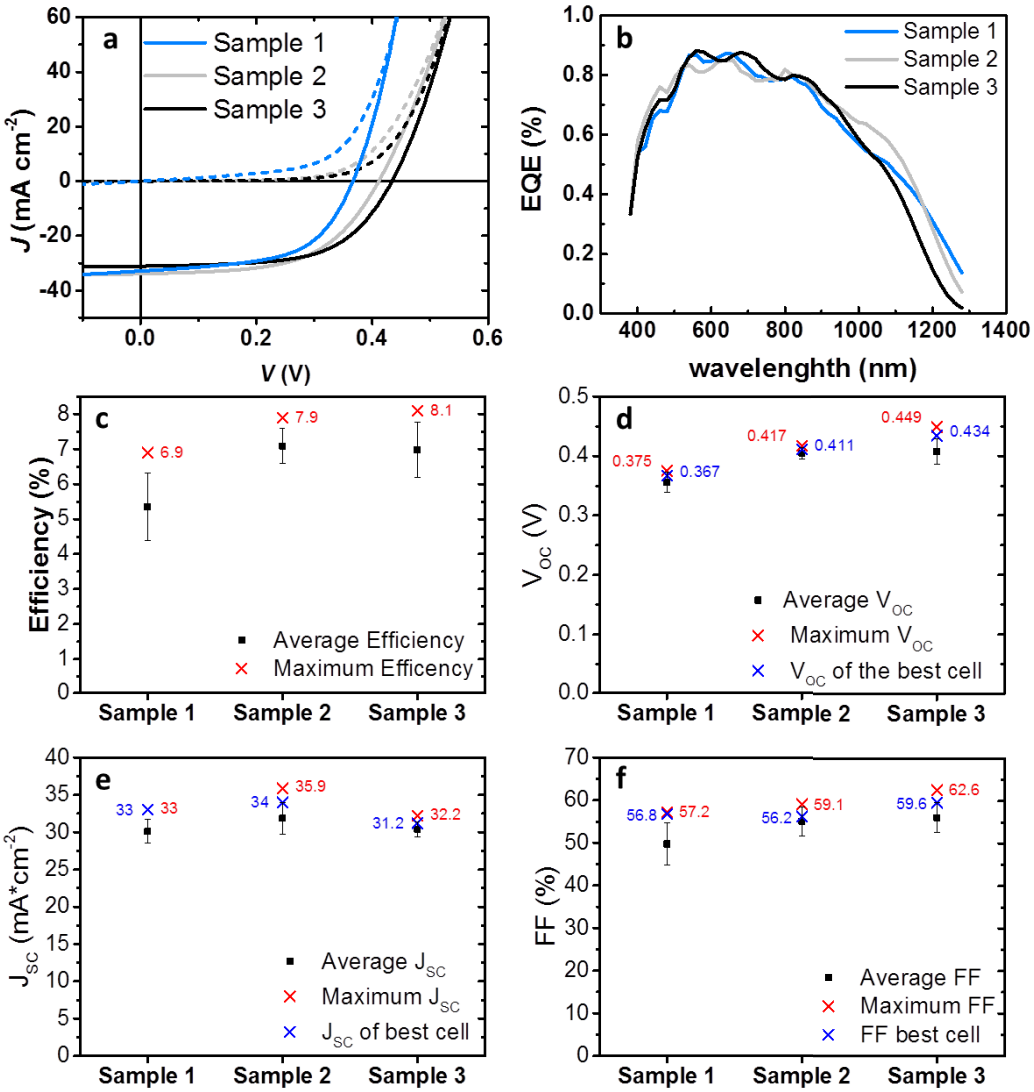

Figure 5. a) Current density – voltage (JV) curves and b) EQE of the best solar cells of each sample of this study. c), d), e), and f) show a summary of the average and standard deviation of the main optoelectronic parameters for the different devices (based on an average of 9 representative cells). Maximum values and the values for the best cells (highest efficiency) of each sample are also represented.

Table 1. Compositional atomic metal ratios of the Cu-Zn-Sn and CZTSe absorber layers of the study presented. The technique used for measuring the composition is specified at the top of each column.

	[XRF-Precursors]		[XRF-CZTSe]		[EDX-CZTSe]	
Sample	**Cu/(Zn+Sn)**	**(Zn/Sn)**	**Cu/(Zn+Sn)**	**(Zn/Sn)**	**Cu/(Zn+Sn)**	**(Zn/Sn)**
Sample 1	0.90	1.03	0.99	1.04	0.86	1.00
Sample 2	0.70	1.09	0.80	1.18	0.75	1.17
Sample 3	0.65	1.12	0.72	1.28	0.66	1.24

499

500 **Table 2.** J-V characteristics of the best CZTSe solar cells fabricated with different
501 compositions. The values of J_{SC} between parenthesis are calculated from the integration
502 of the EQE with the AM 1.5 solar spectrum. The efficiency values are calculated form
503 the measured values of J_{SC}.

Sample	Voc (mV)	Jsc (mA/cm^2)	FF (%)	Eff (%)	Eg (eV)
Sample 1	367	33.0 (33.3)	56.8	6.9	1.00
Sample 2	411	34.0 (34.1)	56.2	7.9	1.04
Sample 3	434	31.2 (32.8)	59.6	8.1	1.07

504